Available online at www.sciencedirect.com
ScienceDirect
Journal of Power Sources 163 (2006) 125–134
JOURNAL OF POWER SOURCES
www.elsevier.com/locate/jpowsour

First-principle molecular-dynamics study of hydrogen adsorption on an aluminum-doped carbon nanotube

Hiroshi Nakano, Hirokazu Ohta, Akira Yokoe, Kentaro Doi, Akitomo Tachibana *

Department of Micro Engineering, Kyoto University, Kyoto 606-8501, Japan

Received 23 August 2005; received in revised form 15 March 2006; accepted 6 April 2006
Available online 9 June 2006

Abstract

We examined first-principle calculation to investigate hydrogen adsorption mechanism on a carbon nanotube (CNT) in which aluminum nanowire was wrapped. The adsorbed hydrogen atoms were stabilized on inner and outer walls of the Al-doped CNT. Hydrogen chemisorptions occurred on inner and outer sides of the Al-doped CNT with 2.81 and 2.93 eV of the binding energy, respectively. These energies were larger than those of the CNT without Al atoms. We also carried out the molecular dynamics (MD) simulations and found that a H atom doped in the Al-doped CNT moved along the axis when a H atom had more than about 4 eV of the kinetic energy. Furthermore the adsorption and desorption mechanism of a H_2 molecule on the CNT surface was studied by the MD simulation. The electronic properties of the systems described above were discussed in terms of quantum energy densities.

Keywords: First-principle calculation; Molecular dynamics; Hydrogen adsorption; Carbon nanotube (CNT); Aluminum; Quantum energy density

1. Introduction

Carbon nanotubes (CNTs) have drawn much attention since they were found at first in 1991 [1] because of their marvelous structure, nanometer dimension, high stability, and excellent conductivity or semiconductivity [2]. Young's moduli of CNT are known as more than 1 TPa [3–5], and their radius and chiralities control the electronic properties such as band gaps [6–10]. In particular, a great interest in CNTs as effective hydrogen-storage materials for fuel-cell applications has recently increased. A lot of experimental [11–17] and theoretical [18–32] reports have been published. Some experimental results reported that CNTs could be covered with hydrogen species: Dillon et al. succeeded to contain hydrogen molecules (H_2) in single-walled CNTs from 5 to 10 wt.% at 133 K and 300 Torr [11], and Chen et al. reported lithium and potassium-doped CNTs could absorb hydrogen from 14 to 20 wt.% at the moderate pressure and room temperature [12]. According to these results, metallic species such as alkali metals are known as effective ones to change the electronic structure of CNTs [16]. Reviews of experimental results are shown in Refs. [13,14]. On the other hand, theoretical studies showed that surfaces of CNTs were occupied by sp^2 hybridized orbitals and π electrons and that this fact would cause the potential barrier to hydrogen adsorption [25,32]. Gülseren et al. investigated adsorption of H and metallic atoms on CNT and reported that charge transfer form metallic atoms or H atoms to CNT was effective to stabilize the systems [21]. Furthermore, they calculated the binding energy of hydrogen adsorption as a function of radius of CNTs [28]. Theoretical studies on hydrogen adsorption on CNTs were summarized by Froudakis in Ref. [25]. Recently some reports have described obvious agreements between experimental results [15–17] and first-principle calculations [26,32].

As a novel nano-structured hydrogen-storage material, we studied aluminum (Al) nanowires, which had great potential of hydrogen adsorption [33]. The surfaces of bare Al nanowires, however, are not so stable that not only hydrogen but also other species will be absorbed [34]. To control the instability of the surfaces of Al nanowires, we suggested a structure such as Al nanowires wrapped in CNT and investigated the electronic properties of them in our previous paper [35].

In this paper, we have extended our study on dynamic aspects of the hydrogen adsorption on an Al-doped CNT introduced in Ref. [35], using first-principle electronic structure calculations.

* Corresponding author. Tel.: +81 75 753 5184; fax: +81 75 753 5184.
E-mail address: akitomo@scl.kyoto-u.ac.jp (A. Tachibana).

0378-7753/$ – see front matter © 2006 Elsevier B.V. All rights reserved.
doi:10.1016/j.jpowsour.2006.04.023

2. Computational details

Fig. 1 shows an imaginary model of (8,0) zigzag CNT in which an Al nanowire is wrapped. The optimized diameter of this CNT is 6.28 Å and the Al nanowire is the most stable on the central axis of the CNT, which was confined in our previous paper [35]. The supercell has orthorhombic system where $a = b = 16.00$ Å and $c = 4.22$ Å as shown in Fig. 1(a) and 32 C atoms and one Al atom are contained in it. In this study, we discuss the effect of Al nanowire wrapped in the CNT on hydrogen adsorption by means of a potential energy surface (PES) analysis and MD simulation.

Electronic structures under the periodic boundary condition were calculated by density functional theory (DFT) with plane-wave basis set and the energy cutoff was taken up to 680 eV (50 Ry). The generalized-gradient approximation formulated by Perdew and Wang [36,37] was used for exchange–correlation interactions, and Hamann's norm-conserving pseudopotentials [38] were adopted for each atom. In each electronic-structure computation, the sampled k point was limited only Γ point.

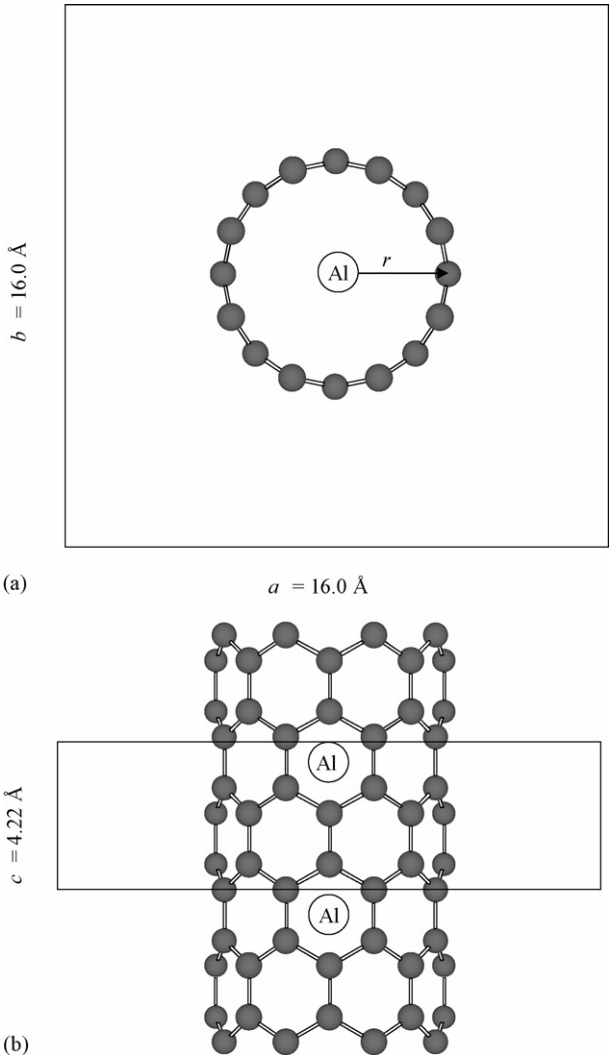

Fig. 1. Super cell of (8,0) zigzag CNT in which Al wire is wrapped and cell parameters: cross-sections (a) perpendicular to and (b) parallel to the c-axis.

In the procedure of MD simulations whose results are discussed in the Section 3.2, Newton's equation of motion was solved using Verlet method as follows [39]:

$$\vec{r}(t+\delta t) = \vec{r}(t) + \delta t\vec{v}(t) + \frac{2}{3}\delta t^2\vec{a}(t) - \frac{1}{6}\delta t^2\vec{a}(t-\delta t), \quad (1)$$

$$\vec{v}(t+\delta t) = \vec{v}(t) + \frac{1}{3}\delta t\vec{a}(t+\delta t) + \frac{5}{6}\delta t\vec{a}(t) - \frac{1}{6}\delta t\vec{a}(t-\delta t), \quad (2)$$

where the forces on atoms were derived from Feynman's formulation [40] by carrying out first-principle calculations. Eqs. (1) and (2) were solved iteratively with the time step δt of atomic motions. In the Section 3.3, we discuss the results solved using another Verlet method as follows:

$$\vec{r}(t+\delta t) = 2\vec{r}(t) + \delta t^2\vec{a}(t) - \vec{r}(t-\delta t), \quad (3)$$

$$\vec{v}(t+\delta t) = \vec{v}(t) + \frac{1}{3}\delta t\vec{a}(t+\delta t) + \frac{5}{6}\delta t\vec{a}(t) - \frac{1}{6}\delta t\vec{a}(t-\delta t). \quad (4)$$

Electronic interactions in each model were analyzed in terms of the quantum energy density based on the regional density functional theory [41–47]. In this paper, we discuss the electronic kinetic energy density [41–44]:

$$n_T(\vec{r}) = \frac{1}{2}\sum_i \nu_i \left(\left\{ -\frac{\hbar^2}{2m}\Delta\psi_i^*(\vec{r}) \right\} \psi_i(\vec{r}) + \psi_i^*(\vec{r}) \left\{ -\frac{\hbar^2}{2m}\Delta\psi_i(\vec{r}) \right\} \right), \quad (5)$$

and the electronic tension density [33–36], $\vec{\tau}^S(\vec{r}) = (\tau^{S1}(\vec{r}), \tau^{S2}(\vec{r}), \tau^{S3}(\vec{r}))$, as follows:

$$\tau^{Sk}(\vec{r}) = \frac{\hbar^2}{4m}\sum_i \nu_i \left(\psi_i^*(\vec{r})\frac{\partial\Delta\psi_i(\vec{r})}{\partial x^k} - \frac{\partial\psi_i^*(\vec{r})}{\partial x^k}\Delta\psi_i(\vec{r}) + \frac{\partial\Delta\psi_i^*(\vec{r})}{\partial x^k}\psi_i(\vec{r}) - \Delta\psi_i^*\frac{\partial\psi_i(\vec{r})}{\partial x^k} \right), \quad (6)$$

for $k = 1$, 2, and 3. Furthermore the electronic stress tensor density [45,46], $\overleftrightarrow{\tau}^S(\vec{r}) = (\tau^{Skl}(\vec{r}))$, as follows:

$$\tau^{Skl}(\vec{r}) = \frac{\hbar^2}{4m}\sum_i \nu_i \left(\psi_i^*(\vec{r})\frac{\partial^2\psi_i(\vec{r})}{\partial x^k\partial x^l} - \frac{\partial\psi_i^*(\vec{r})}{\partial x^k}\frac{\partial\psi_i(\vec{r})}{\partial x^l} + \frac{\partial^2\psi_i^*(\vec{r})}{\partial x^k\partial x^l}\psi_i(\vec{r}) - \frac{\partial\psi_i^*(\vec{r})}{\partial x^l}\frac{\partial\psi_i(\vec{r})}{\partial x^k} \right), \quad (7)$$

for $\{k, l\} = \{1, 2, 3\}$ where m is the mass of an electron, and $\psi_i(\vec{r})$ and ν_i are the electron wave function and occupation number of the ith state, respectively. $n_T(\vec{r})$ divides the space into the electronic drop region R_D ($n_T(\vec{r}) > 0$) where valence electrons can move freely in the meaning of classical mechanics and the electronic atmosphere region R_A ($n_T(\vec{r}) < 0$) where electrons can move according to the quantum mechanical effect. $\vec{\tau}^S(\vec{r})$ shows the force on the electron density due to the kinetic energy density. In the stationary state, this force density is in balance

with the electronic external force density, Lorentz force density, because the total electronic force density is equal to zero at each point. The positive and negative eigenvalues of $\overleftrightarrow{\tau}^{S}(\vec{r})$ represent the tensile and compressive stress, respectively, and this plot reveals the properties of chemical bonds [45,46]. In this paper we show the largest component of the eigenvalues and eigenvectors of stress tensor density. All of computational methods in this paper have been implemented in Periodic Regional DFT program package [47].

3. Results and discussion

3.1. Potential energy surfaces

First, we calculated the PESs with respect to a H atom around the Al-doped CNT and pristine (8,0) zigzag CNT, and these results were shown in Figs. 2 and 3, respectively. Four cross-sections were sampled as shown in Fig. 2(a), denoted as I through IV, and the total energies were calculated on the surfaces. As a result, continuous stable regions extended round the centered Al atom inside the nanotube. This result denotes H atoms strongly interact with Al atoms even in the CNT. On the other hand, outside the CNT, a H atom tended to be bound on one of C atoms composed of the wall although a H atom did not seem to be absorbed inside the wall. It was considered from these results that, because of the convex curve of the wall, electrons composed of $2p\pi$ delocalized orbitals on the carbon network appeared to be localized on each C atom and induced rehybridization of them to sp^3 orbitals. The properties of C–H bonds on CNT, strengthened by the change of the electronic structure of the carbon network, were discussed by some other groups [15,21,24]. Fig. 3 shows PESs of a H atom close to inner and outer walls of the pristine CNT, drawn by the same way as those of the Al-doped CNT. Outside the CNT wall, the H atom tended to adsorb on C atoms but it was not as strong as the adsorption on the Al-doped CNT. Inside the wall, although there are a few stable points of a H atom, the H atom tends to repulsively interact with C atoms. This picture is contrary to the C–H bond outside the wall and denotes the convex structure of CNT is effective for hydrogen adsorption.

Fig. 4 shows the energy diagrams of the electronic state calculation. Fig. 4(a) shows that the pristine CNT is stabilized by a H adatom and the H atom is more stable on the outer wall than on the inner wall. The binding energy E_b of the H atom on the two kinds of CNT is defined as follows:

$$E_b = E_{CNT,(Al)} + E_H - E_{CNT,(Al),H}, \quad (8)$$

where $E_{CNT,(Al)}$, E_H, and $E_{CNT,(Al),H}$ denote total energies of the Al-doped CNT or pristine one, H atom, and whole system, respectively. Outside the CNT, E_b was estimated to be 2.56 eV, and inside it, E_b was 1.27 eV in the vicinity of C atoms. As shown in Fig. 4(b), when the H atom was bound on a C atom of the Al-doped CNT, the system was more stabilized and E_b was 2.93 eV. This means that Al atoms influence the binding energy of C–H bond on the wall and make the system more stable. Inside the nanotube, a H and Al atoms made a chemical bond and this caused the drastic increase of E_b up to 2.81 eV although to wrap Al atoms in the CNT was endothermic by 0.37 eV as shown in Fig. 4(c). However the interaction between a H and Al atoms where E_b was estimated as 4.18 eV was so strong that the Al atom was effective enough to hydrogen adsorption on each side of the CNT.

3.2. Molecular dynamics simulation of a hydrogen atom on the inner wall of (8,0) CNT

We carried out MD simulations to discuss the motion of activated H atoms in the (8,0) CNT. In this section, the dynamic aspects of hydrogen adsorption and desorption are shown, comparing with the static properties described above. In the MD simulations, at starting point, a H atom was located on one of the most stable points in the Al-doped CNT and activated by the kinetic energy, 3, 4, and 5 eV. The directions of the initial momenta were decided at random. The C and Al atoms were fixed at the optimized positions in a series of the simulations, and the total energies given at the starting point were conserved by our original scaling method [48–51]. The time step δt used to solve the equations of motion, Eqs. (1) and (2), was set to 2.0 fs in the numerical differential procedure. Fig. 5 shows the trajectories of the H atom projected on a cross-section parallel to the c-axis of the CNT. The H atom was trapped in the potential well caused by the Al atom and could not leap over the well when it was excited within 3 eV of its kinetic energy. When the activation energy reached to 4 eV, the H atom could jump over the potential wall and run along the Al wire. In the MD

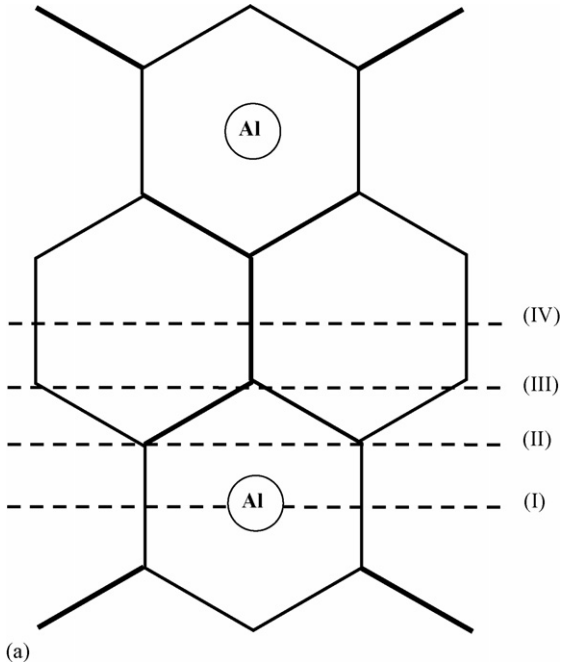

Fig. 2. (a) Four layers, (I), (II), (III), and (IV), on which PESs are calculated and PESs, (b), (c), (d), and (e), corresponding to the four layers from (I) to (IV), respectively. Rings with gray line denote out lines of the CNT. A mark, "×", shown in (b) is one of the most stable points. The interval between each layer is 1 Å.

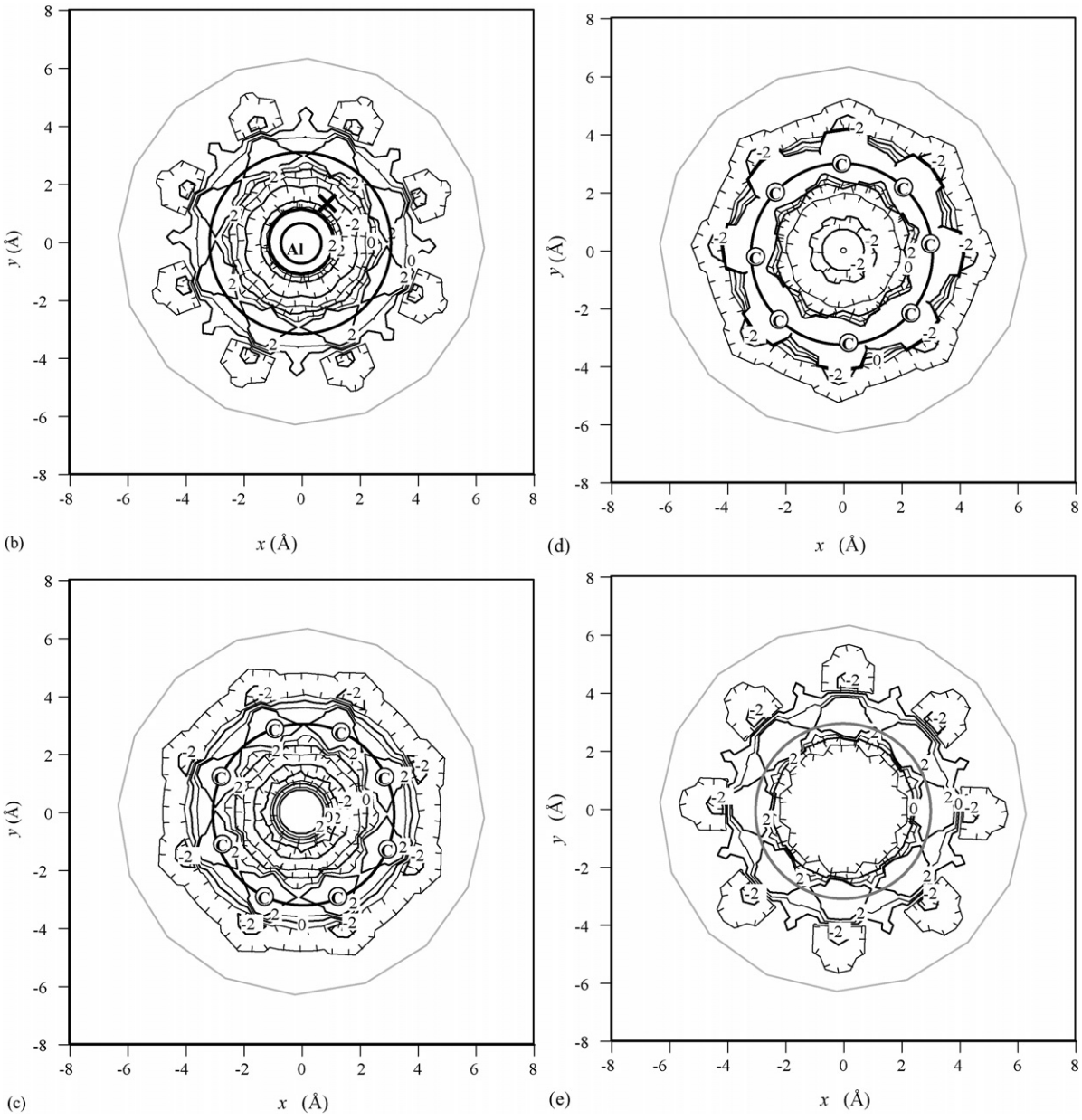

Fig. 2. (*Continued*).

simulations, it is difficult for the H atom to run through the minimum energy paths as calculated by PESs because the thermally excited atoms collided with other atoms and were scattered in the various directions. Fig. 6 shows the potential energy transitions corresponding to the trajectories shown in Fig. 5. The more drastic change of the potential energy was appeared when the H atom initially got 5 eV of its kinetic energy. The higher kinetic energy was given, the more frequently the H atom collided with the potential walls. In this study, the Al and C atoms were fixed and only the H atoms could move freely. Comparing between the results of MD simulations and PESs described above, it is obvious to transport H atoms smoothly in the nanotubes the thermal excitation is required more in the real system than in the ideal PESs.

3.3. Molecular dynamics simulation of a hydrogen atom on the outer wall of (8,0) CNT

Next, we discuss the hydrogen adsorption on the outside of the Al-doped CNT and pristine one. In this simulation, all of Al and C atoms were released from the constraints as well as a H atom. The time step δt was set to 2.5 fs. In case of the simulation on the pristine CNT, a H atom was located at a point 6.00 Å away from the central axis of the nanotube, and its momentum was initially set to zero. The distances from the H atom to the center of mass of the CNT and to the surface of the CNT are plotted as a function of time in Fig. 7. The H atom oscillated around 5 Å from the center of mass of the CNT and quivered within the range from 0.5 through 1 Å away from the surface. In case of the

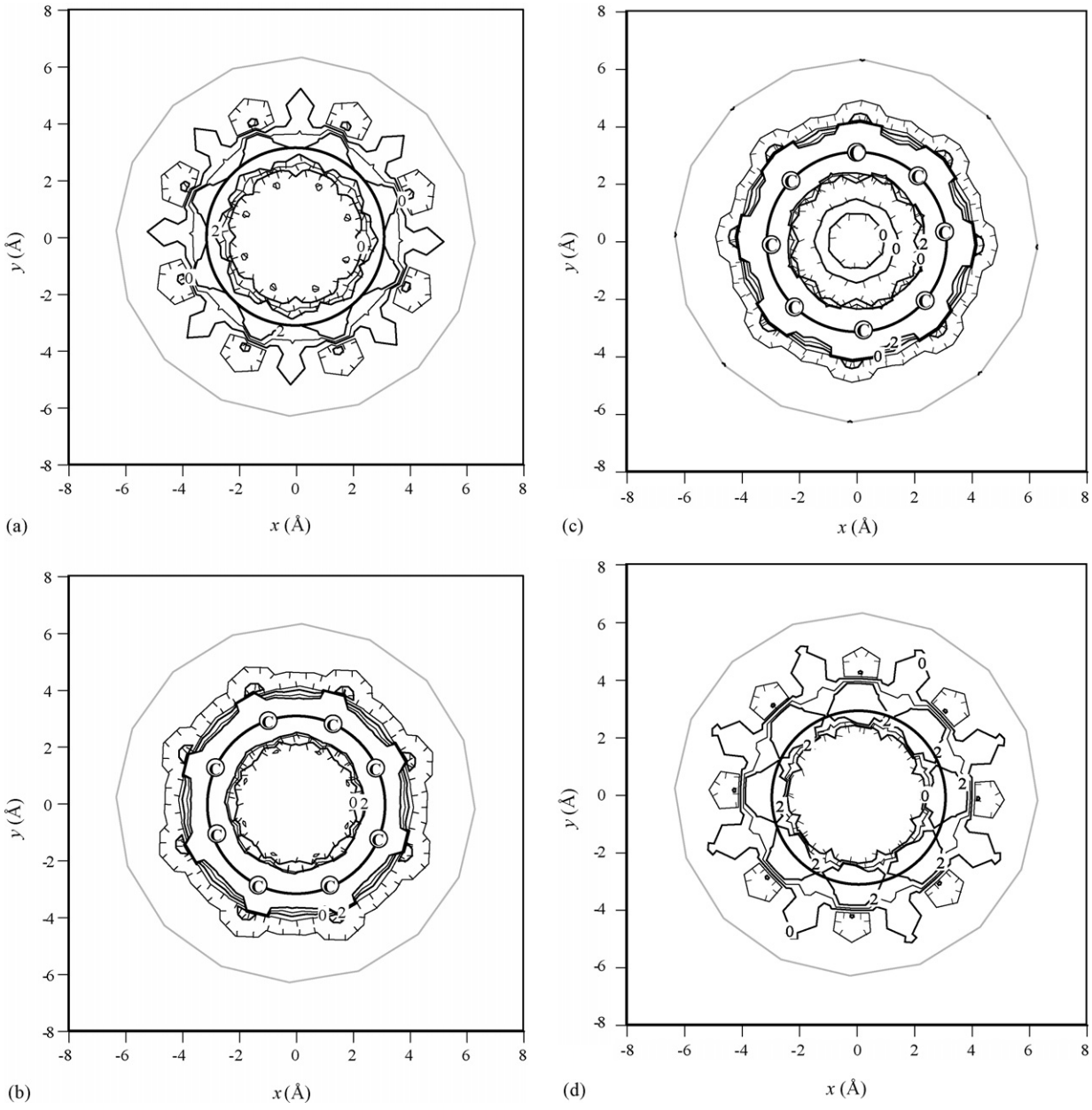

Fig. 3. PESs of a H atom in the pristine CNT, (a), (b), (c), and (d), corresponding to the four layers shown in Fig. 2(a).

Al-doped CNT, the initial position of a H atom was set to 5.41 Å from the central axis of the CNT and the Al atom was initially on the central axis. Fig. 8 shows the plots of the distances between the H atom and the Al-doped CNT in a similar manner to Fig. 7. In this case, the H atom quivered on the surface in the same way as on the pristine CNT but the Al wire seemed to suppress the distortion of the CNT. The oscillation between the H atom and the center of mass of the Al-doped CNT appeared to be calm comparing Fig. 7(a) with Fig. 8(a).

Furthermore the effect of the Al wire to suppress the distortion of the CNT is revealed by calculating the dispersion of the CNTs as follows:

$$\left\langle \Delta r^2 \right\rangle = \sum_{i=1}^{N} |\vec{r}_i - \vec{r}_{0i}|^2, \tag{9}$$

where N is the number of C atoms and $\vec{r}_i$ and $\vec{r}_{0i}$ denote the positions of the ith C atom as a function of time and at time zero, respectively. The origin of these position vectors was the center of mass of the CNT at each time. This quantity as a function of time, as shown in Fig. 9, estimates the dispersion of the CNT from the initial structure. It was clarified that the pristine CNT was strained more markedly by the H atom than the Al-doped CNT and the Al wire controlled the transformation of the CNT. In this simulation, however, the Al atom did not seem to affect the motion of the H atom.

Snapshots picked up at 500 and 800 fs during the MD steps for the Al-doped CNT are shown in Fig. 10. At 500 fs, the H atom outside the CNT was located at 0.69 Å away from the nearest C atom and 5.60 Å from the Al atom inside the CNT. While at 800 fs, the H atom was at 0.71 Å away from the nearest C atom

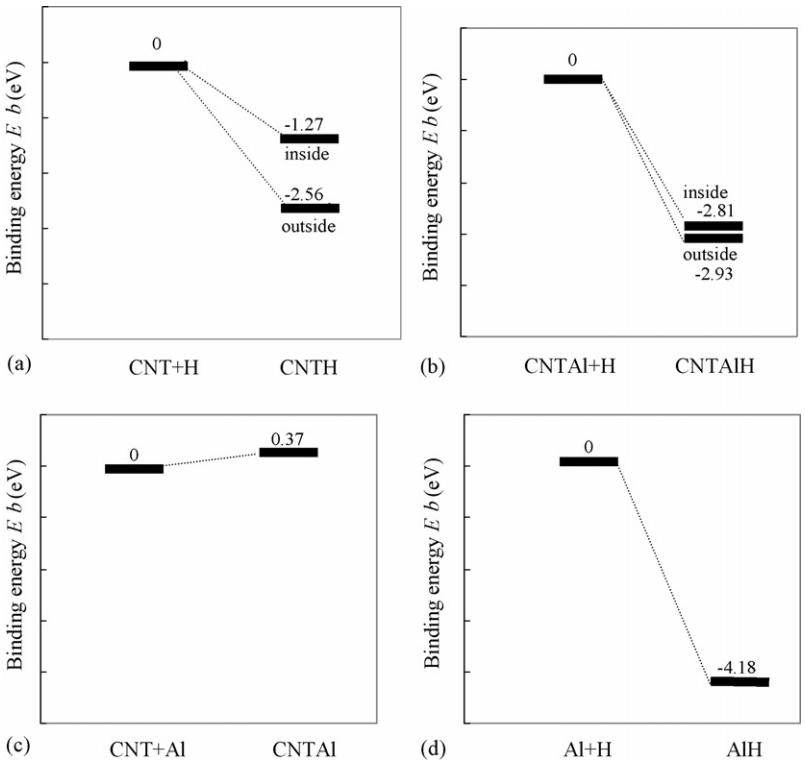

Fig. 4. Relative-energy diagrams of the binding energy: (a) and (b) a H atom on outer and inner walls of the pristine CNT and Al-doped CNT, respectively, (c) an Al atom in the pristine CNT, and (d) a H atom on the Al wire.

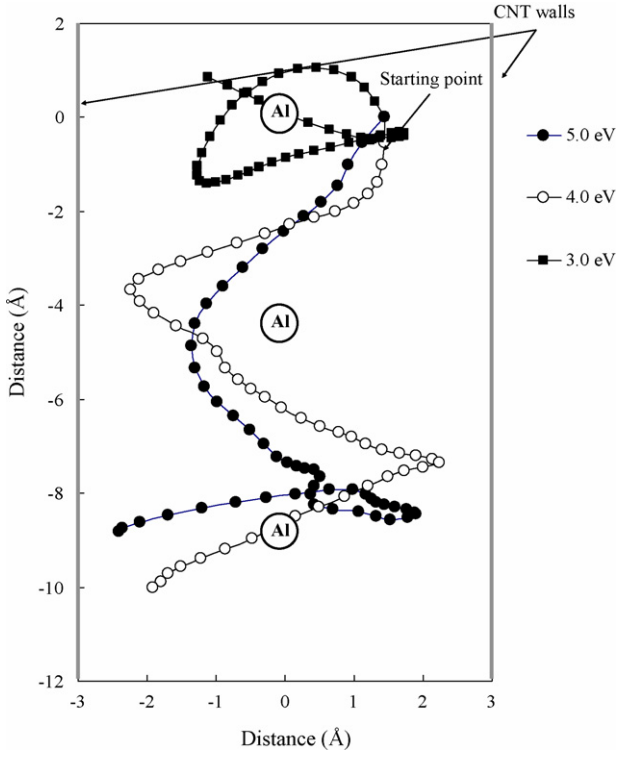

Fig. 5. Trajectories of a H atom in the Al-doped CNT during the MD simulations. The H atom initially had 3.0, 4.0 and 5.0 eV of the kinetic energy and was located at the most stable point in Fig. 2(b).

and 3.25 Å from the Al atom. We paid attention to these two points when the H atom was close to the wall but the distances between the H and Al atoms did not seem to be correlated. The binding energies of these two were given by 4.40 eV at 500 fs and 3.92 eV at 800 fs and these values were larger, by over 1 eV, than the energy estimated by PES analysis in the previous section. In addition, we calculated the binding energies of the same geometry without the Al atom, and the values were given by 3.48 eV at 500 fs and 2.48 eV at 800 fs. These results show that the binding energies of the H atom at 500 and 800 fs were not so different, but the existence of Al atom affected the binding energy and especially the point at 800 fs where the distance between the H and Al atoms was short.

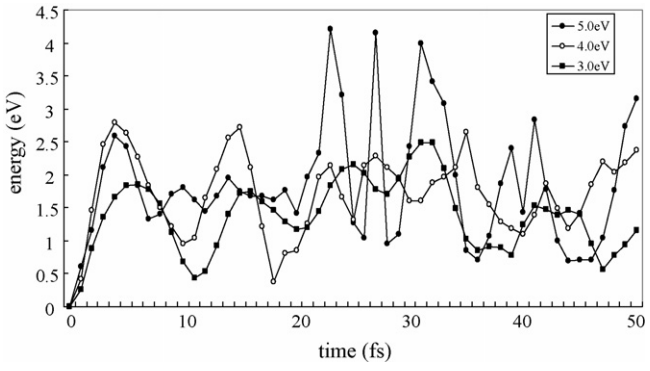

Fig. 6. Transitions of each potential energy corresponding to the trajectories in Fig. 5.

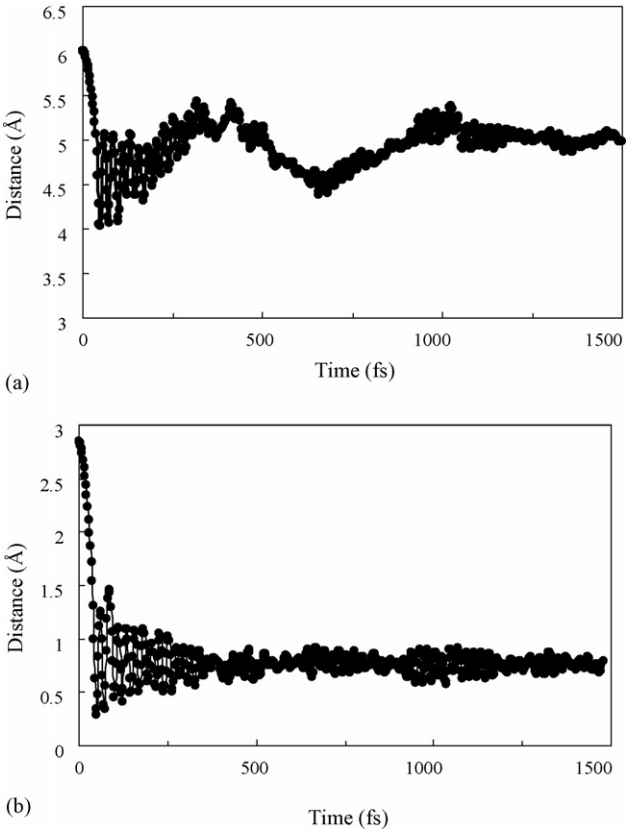

Fig. 7. Transitions of distances during the MD simulation: (a) distance between the H atom and the center of mass of the pristine CNT and (b) that from the H atom to the surface of the CNT.

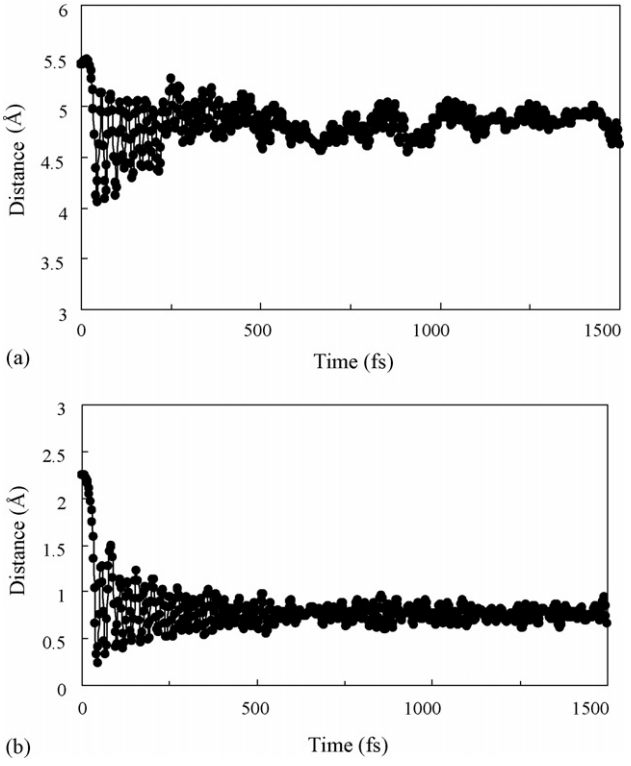

Fig. 8. Transitions of distances during the MD simulation: (a) distance between the H atom and the center of mass of the Al-doped CNT and (b) that from the H atom to the surface of the CNT.

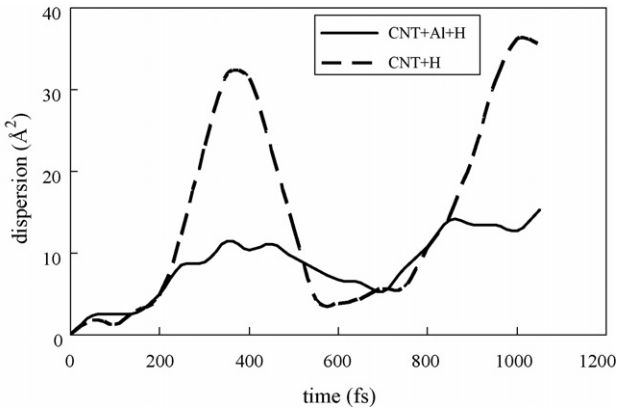

Fig. 9. Dispersion of the CNTs described as $\langle \Delta r^2 \rangle$. The solid line and the dotted line denote the dispersions of the Al-doped CNT and pristine CNT, respectively.

3.4. Molecular dynamics simulation of a hydrogen molecule

Next, we show the results of MD simulations of a H_2 molecule on the Al-doped CNT. At the starting point, the center of mass of a H_2 molecule was located at 4.16 Å from the central axis of the CNT and several values of the length between two H atoms were attempted to excite its oscillation. In these simulations, the time step of the atomic motion was set to 1.0 fs. Fig. 11(a) shows the transitions of the potential energy as a function of time, and (b) and (c) stable structures after some steps corresponding to the first and second attempts, respectively. When the bond length of a H_2 molecule was 0.97 Å at the initial position corresponding to the first attempt, the H_2 molecule was firstly attracted to the wall, collided with the wall, and left away from the CNT as a molecule. In case of the second attempt, when the distance

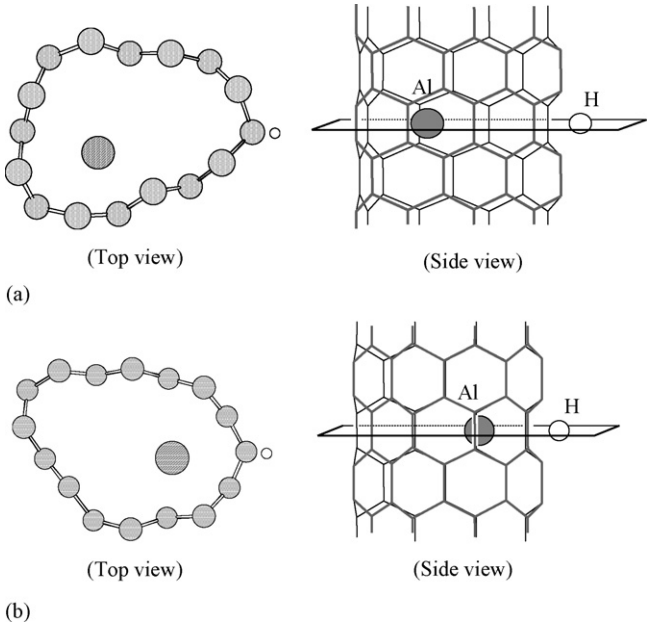

Fig. 10. Snapshots at (a) 500 and (b) 800 fs during the MD simulation. At 500 fs, the H atom was 0.69 Å away from the wall of the CNT, and at 800 fs, the H atom 0.71 Å away from the wall.

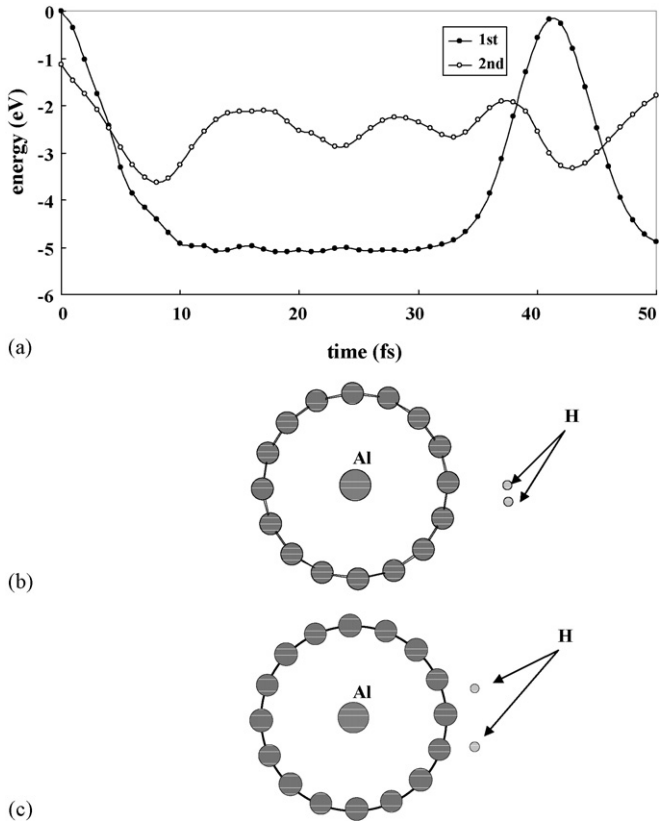

Fig. 11. (a) Potential-energy transition during the MD simulation in which a H_2 molecule interacted with Al-doped CNT. (b) The snapshot at 50 fs corresponding to the first trial. When the bond length was initially 0.97 Å, a H_2 molecule collided against the CNT surface and left from it. (c) The snapshot at 50 fs corresponding to the second trial. When the bond length was stretched to 1.7 Å, a H_2 molecule was resolved into two H atoms and then adsorbed on the surface.

between two H atoms got longer to 2.0 Å at the starting point, two isolated H atoms adsorbed on the C atoms. This is because a H_2 molecule gets stable as H atoms approach the surface of the CNT. It was calculated that a H_2 molecule which had 2.0 Å of the bond length was more stable on the CNT by 1.1 eV than that which had 0.97 Å of the length. It was clarified from these results that some activation energy was required to dissociate a H_2 molecule to two H atoms to adsorb them on the CNT. We, however, have not investigated the details of the reaction path of the hydrogen adsorption process yet. Lee et al. estimated the potential barrier required for dissociative adsorption of a H_2 molecule on (5,5) CNT as between 2.70 and 3.07 eV [27].

3.5. Quantum energy density

We discuss electronic states of the most stable structure of the Al-doped and pristine CNT. We analyzed those electronic structures in terms of electron energy density, e.g. kinetic energy density, tension density, and stress tensor density [41–46]. Figs. 12 and 13 show these densities picked out from the cross-sections along the *c*-axis on which C, H, and Al atoms are located. From these electron-energy-density plots it was found that H atoms made covalent bond with Al and C atoms in the stable states.

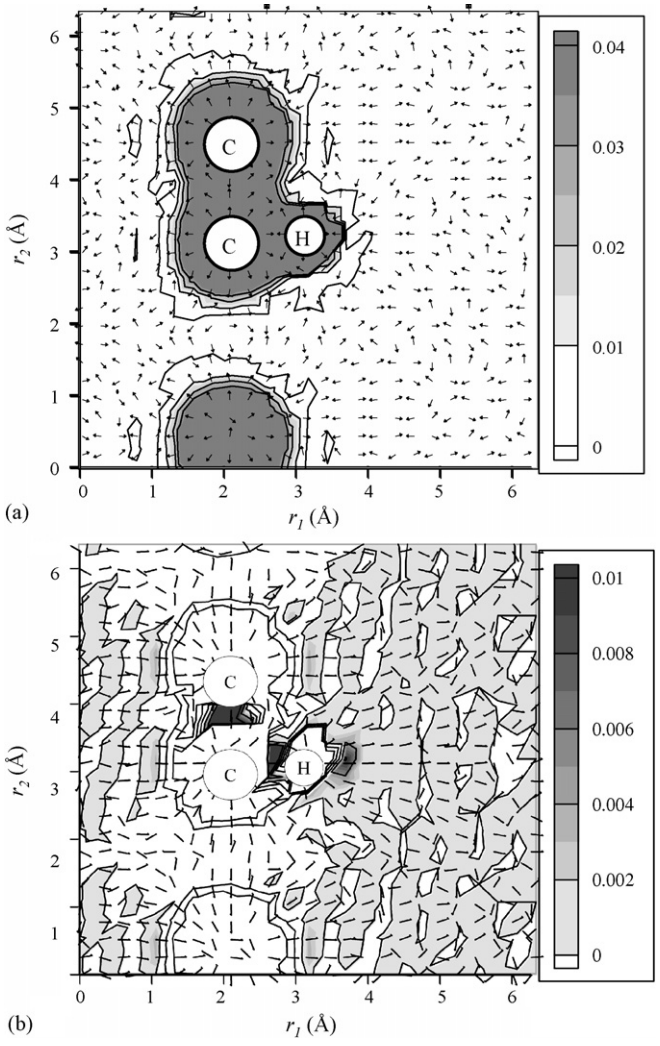

Fig. 12. Contour maps of energy density at the most stable configuration of a H atom on the pristine CNT. (a) The kinetic energy density $n_T(\vec{r})$ of a cross-section on which the H and C atoms exist. R_D is shown by contour lines and gray-scale gradation. The tension density $\vec{\tau}^S(\vec{r})$ is also shown by vectors. (b) Contour maps of the stress tensor density $\overleftrightarrow{\tau}^S(\vec{r})$ whose positive values are represented by gray scale. Short lines denote eigenvectors of $\overleftrightarrow{\tau}^S(\vec{r})$.

Fig. 12(a) shows the distribution of the kinetic energy density $n_T(\vec{r})$ in a system of the pristine CNT and H atom. The electronic drop region R_D, where electronic kinetic energy density presents plus value wrapped a H and C atoms. This means electrons between the H and C atoms can be exchanged without tunneling between these atoms. The tension density $\vec{\tau}^S(\vec{r})$ shown by vectors represents the force density caused by electron kinetic energy density and this force density is in balance with Lorentz force density in the equilibrium state. Fig. 12(b) shows the largest eigenvalues of the stress tensor density $\overleftrightarrow{\tau}^S(\vec{r})$ and those eigenvectors represented by short lines. The tensile stress represented by plus values appears between the H and C atoms and this means the generation of covalent bonds between these atoms. One of the interesting properties of the tensile stress is that spindle structures appear between two atoms bonding covalently, as clearly shown in Fig. 12(b). Fig. 13 shows the

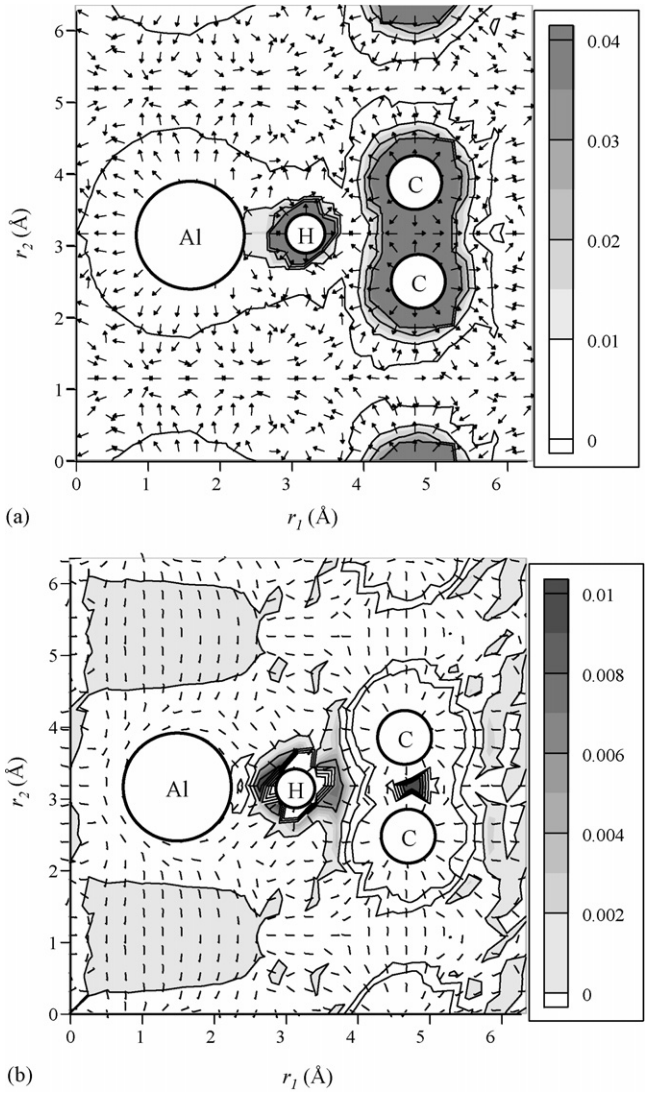

Fig. 13. Contour maps of energy density at the most stable configuration of a H atom in the Al-doped CNT. (a) The kinetic energy density and tension density and (b) the stress tensor density are represented in the same way as Fig. 11. In this case, the H, C, and Al atoms are located on the same plane.

kinetic energy density and the stress tensor density where a H atom is in the Al-doped CNT and H, Al, and C atoms are on the same plane. The kinetic energy density is dense between not only H and C atoms but also H and Al atoms. Electrons can be exchanged between these atoms. The stress tensor density shown in Fig. 13(b) shows covalent bonds and spindle structures between Al–H as well as C–H. These results attribute to the stability of the systems in which the H atom adsorbs on the pristine CNT or Al-doped one.

4. Conclusions

In this paper, we studied hydrogen adsorption mechanism on (8,0) carbon nanotube with Al dopant. Electronic structures of the models were computed using DFT method with pseudopotentials, and MD simulations based on the first-principle calculation were carried out to understand the dynamical properties of the hydrogen adsorption and desorption on the CNT. The potential energy analysis gave the result that in the Al-doped CNT the H atom stabilized not close to the C atoms but around the Al atom with the binding energy of 2.81 eV, and on the outer wall it stabilized the most just above a C atom of the CNT with that energy of 2.93 eV. On the other hand, the binding energies of a H atom were 1.27 and 2.56 eV at inside and outside of the pristine CNT, respectively. This result concludes that hydrogen is more stable in the vicinity of CNT with Al dopant than pristine one.

We found that a H atom contained in Al-doped CNT ran along the axis direction when the H atom activated by 4 eV of the kinetic energy at the most stable point. It was difficult for a H atom to pass through the lowest potential barrier because PESs had narrow valley as shown in Fig. 2.

An Al atom and (8,0) CNT were activated by the vibration of a H atom on the CNT surface, and the H atom was settled at within the range from 0.5 to 1 Å on the surface. The binding energy of the hydrogen adsorption was influenced by the Al atom when the distance between the Al and H atoms was short. It was found that the Al atom changed electronic structure of the pristine CNT and suppressed the deformation of it. Therefore the activated Al atom has an important role for the motion of the H atom in the vicinity of the CNT.

We also studied the desorption mechanism of a H_2 molecule on the Al-doped CNT. By means of the MD simulations based on first-principle calculation, a H_2 molecule left away from the nanotube when the length between two H atoms was 0.97 Å, while two H atoms bonded to the C atoms when the bond length stretched to 1.7 Å.

Furthermore, we analyzed the properties of electrons in terms of quantum energy densities [41–46]. These density plots can give more information about electronic interactions between atoms. The large adsorption energy of a H atom on the Al-doped CNT was reflected by the interaction between the Al and H atoms as well as the covalent bond between the H and C atoms, represented by spindle structure in terms of the stress tensor density.

Acknowledgements

This paper was supported in part by Center of Excellence for Research and Education on “Complex Functional Mechanical System” as a COE program of the Ministry of Education, Culture, Science and Technology, Japan, for which the authors express their gratitude. A part of the computations was carried out by Fujitsu Primepower HPC2500 in Academic Center for Computing and Media Studies, Kyoto University.

References

[1] S. Iijima, Nature (London) 354 (1991) 56.
[2] R. Saito, G. Dresselhaus, M.S. Dresselhaus, Physical Properties of Carbon Nanotube, Imperial College Press, London, 1998.
[3] S. Ogata, Y. Shibutani, Phys. Rev. B 68 (2003) 165409.
[4] J.P. Lu, J. Phys. Chem. 58 (1997) 1649.
[5] J.P. Lu, Phys. Rev. Lett. 79 (1997) 1297.
[6] N. Hamada, S. Sawada, A. Oshiyama, Phys. Rev. Lett. 68 (1991) 1579.
[7] T.W. Odom, J.-L. Huang, P. Kim, C.M. Lieber, J. Phys. Chem. 104 (2000) 2794.

[8] J.W. Ding, X.H. Yan, J.X. Cao, Phys. Rev. B 66 (2002) 073401.
[9] S. Reich, C. Thomsen, P. Ordejón, Phys. Rev. B 65 (2002) 155411.
[10] P.N. D'yachkov, D.V. Makav, Phys. Rev. B 71 (2005) 081101.
[11] A.C. Dillon, K.M. Jones, T.A. Bekkedahl, C.H. Kiang, D.S. Bethune, M.J. Heben, Nature 386 (1997) 377.
[12] P. Chen, X. Wu, J. Lin, K.L. Tan, Science 285 (1999) 91.
[13] A. Züttel, P. Sudan, Ph. Mauron, T. Kiyobayashi, Ch. Emmernegger, L. Schlapbach, Int. J. Hydrogen Energy 27 (2002) 203.
[14] F.L. Darkin, P. Malbrunot, G.P. Tartaglia, Int. J. Hydrogen Energy 27 (2002) 193.
[15] P. Ruffieux, O. Grühiag, M. Bielmann, P. Mauron, L. Schlapbach, P. Gröning, Phys. Rev. B 66 (2002) 245416.
[16] S. Suzuki, F. Maeda, Y. Watanabe, T. Ogino, Phys. Rev. B 67 (2003) 115418.
[17] G. Chiarello, E. Maccallini, R.G. Agostino, T. Caruso, V. Formoso, L. Papagno, E. Colavita, A. Goldoni, R. Larciprete, S. Lizzit, L. Petaccia, Phys. Rev. B 69 (2004) 153409.
[18] V.V. Simonyan, P. Diep, J.K. Jonson, J. Chem. Phys. 111 (1999) 9778.
[19] S.M. Lee, K.S. Park, Y.C. Choi, Y.S. Park, J.M. Bok, D.J. Bae, K.S. Nahm, Y.G. Choi, S.C. Yu, N.-g. Kim, T. Frauenheim, Y.H. Lee, Synth. Met. 113 (2000) 209.
[20] J. Zhao, A. Buldum, J. Han, J.P. Lu, Phys. Rev. Lett. 85 (2000) 1706.
[21] O. Gülseren, T. Yildirim, S. Ciraci, Phys. Rev. Lett. 87 (2001) 116802.
[22] S.-P. Chan, G. Chen, X.G. Gong, Z.-F. Liu, Phys. Rev. Lett. 87 (2001) 205502.
[23] Y. Ma, Y. Xia, M. Zhao, M. Ying, X. Liu, P. Liu, J. Chem. Phys. 115 (2001) 8152.
[24] K. Tada, S. Furuya, K. Watanabe, Phys. Rev. B 63 (2001) 155405.
[25] G.E. Froudakis, J. Phys.: Condens. Matter 14 (2002) R453.
[26] T. Miyake, S. Saito, Phys. Rev. B 65 (2002) 165419.
[27] E.-C. Lee, Y.-S. Kim, Y.-G. Jin, K.J. Chang, Phys. Rev. B 66 (2002) 073415.
[28] O. Gülseren, T. Yildrim, S. Ciraci, Phys. Rev. B 66 (2002) 121401R.
[29] X. Sha, B. Jackson, Surf. Sci. 496 (2002) 318.
[30] G. Lu, H. Scudder, N. Kioussis, Phys. Rev. B 68 (2003) 205416.
[31] J. Li, T. Furuta, H. Goto, T. Ohashi, Y. Fujiwara, S. Yip, J. Chem. Phys. 119 (2003) 2376.
[32] Y. Miura, H. Kasai, W.A. Diño, H. Nakanishi, T. Sugimoto, Jpn. J. Appl. Phys. 42 (2003) 4626.
[33] Y. Kawakami, T. Kikura, K. Doi, K. Nakamura, A. Tachibana, Materials Science Forum, vols. 426–432, 2003, pp. 2399–2404.
[34] T. Makita, K. Doi, K. Nakamura, A. Tachibana, J. Chem. Phys. 119 (2003) 538.
[35] Y. Kawakami, Y. Nojima, K. Doi, K. Nakamura, A. Tachibana, Electrochim. Acta 50 (2004) 735.
[36] J.P. Perdew, Y. Wang, Phys. Rev. B 45 (1992) 13244.
[37] J.P. Perdew, J.A. Chevary, S.H. Vosko, K.A. Jackson, M.R. Pederson, D.J. Singh, C. Fiolhais, Phys. Rev. B 46 (1992) 6671.
[38] D.R. Hamann, Phys. Rev. B 40 (1989) 2980.
[39] M.P. Allen, D.J. Tildesley, Computer Simulation of Liquids, Oxford University Press, New York, 1987, pp. 78–82.
[40] R.P. Feynman, Phys. Rev. 56 (1939) 340.
[41] A. Tachibana, J. Chem. Phys. 115 (2001) 3497.
[42] A. Tachibana, in: S.P. Baker (Ed.), Stress Induced Phenomena in Metallization, American Institute of Physics, New York, 2002, pp. 105–106.
[43] A. Tachibana, in: K.D. Sen (Ed.), Reviews in Modern Quantum Chemistry: A Celebration of the Contributions of Robert Parr, World Scientific, Singapore, 2002, pp. 1327–1366, Chap. 45.
[44] A. Tachibana, in: E.J. Brändas, E.S. Kryachko (Eds.), Fundamental World of Quantum Chemistry: A Tribute to the Memory of Per-Olov Löwdin, vol. 2, Kluwer, Dordrecht, 2003, pp. 221–239.
[45] A. Tachibana, Int. J. Quantum Chem. 100 (2004) 981.
[46] A. Tachibana, J. Mol. Model. 11 (2005) 301.
[47] K. Doi, K. Nakamura, A. Tachibana, Periodic Regional DFT Program Package, Ver. 2, Tachibana Lab., Kyoto University, Kyoto, 2004.
[48] A. Tachibana, M. Fuju, J. Chem. Phys. 110 (1999) 2323.
[49] A. Tachibana, T. Iwai, Phys. Rev. A 33 (1986) 2262.
[50] T. Iwai, A. Tachibana, Ann. Inst. Henri Poincare 70 (1999) 525.
[51] A. Tachibana, J. Mol. Struct. (Theochem) 310 (1994) 1.